Including General Environmental Effects in K-factor Approximation for Rice-Distributed VANET Channels

Craig Cooper[a], Abhinay Mukunthan[a], Farzad Safaei[a], Montserrat Ros[b], Daniel Franklin[c], Mehran Abolhasan[c]

[a] *ICT Research Institute - University of Wollongong, Wollongong NSW 2500, Australia*
[b] *School of Electrical, Computer, and Telecommunications Engineering - University of Wollongong, Wollongong NSW 2500, Australia*
[c] *School of Computing and Communications - University of Technology, Sydney, Broadway NSW 2007, Australia*

Abstract

This paper presents a method of approximating the Ricean K-factor based on the instantaneous static environment. The strongest signal propagation paths are resolved in order to determine specular and diffuse powers for approximation. The model is experimentally validated in two different urban areas in New South Wales, Australia. Good agreement between the model and experimental data was obtained over short-range communication links, demonstrating the suitability of the model in urban VANETs. The paper concludes with recommendations for methods to account for vehicles in the simulation and incorporating additional phenomena (such as scattering) in the approximation.

Keywords: K-factor, Rice Fading, Channel Modelling, Experimental Analysis

1. Introduction

Research into vehicular ad hoc networks (VANETs) is highly dependent on the characteristics of the channel over which they operate. Many VANET protocols and architectures are intended for use in built-up urban environments, which are subject to complex fading and shadowing effects at a variety of time-scales. The presence of vehicles and meteorological phenomena are further complications which need to be taken into account if the real-world behaviour of a proposed VANET system is to be completely understood. Experimental work with VANETs is inherently more challenging compared to other ad-hoc networks, and it is difficult to produce truly representative results without the expenditure of impractical amounts of time and money. Therefore, accurate and flexible simulation tools are of critical importance to any study into VANETs.

Email addresses: craigsco@bigpond.net.au (Craig Cooper), am394@uowmail.edu.au (Abhinay Mukunthan), farzad@uow.edu.au (Farzad Safaei), montse@uow.edu.au (Montserrat Ros), daniel.franklin@uts.edu.au (Daniel Franklin), mehran.abolhasan@uts.edu.au (Mehran Abolhasan)

Urban environments have been traditionally modelled as Rice-distributed channels, characterised by a parameter called the K-factor:

$$K = \frac{A^2}{2\sigma^2} \Rightarrow K_{dB} = 10\log_{10}\left(\frac{A^2}{2\sigma^2}\right) \quad (1)$$

where $A^2/2$ is the power in the specular or line-of-sight component, and σ^2 is the power in the diffuse or multipath components. Often, VANET researchers analyse proposed communication protocols using a constant K-factor, implying a stationary fading scenario [1]. This is an instance of the wide-sense stationary and uncorrelated scattering (WSSUS) assumption, which holds for the well-studied cellular network scenario. It has been widely assumed that this principle is also valid in the VANET channel; however, VANETs differ significantly from cellular networks in terms of antenna heights, frequency range, scattering properties, and level of mobility [2].

Previous experimental work has established that the WSSUS assumption is not generally valid in VANETs [3, 4], and that the K-factor is variable in space and time [5–8]. Empirical studies have shown that the K-factor is significantly dependent on the surrounding environment [7, 9]. A simulation that accounts for this dependence will therefore provide a more accurate demonstration of protocol behaviour than one which assumes WSSUS.

This paper proposes a technique for modelling K-factor dynamics in an urban VANET environment. Rather than statistical analysis of experimental measurements, the model attempts to calculate the propagation paths between source and destination, accounting for local building geometry and materials to reflect the influence of the instantaneous local signal propagation environment. The model is validated through experiments conducted in traffic in a variety of urban environments in New South Wales, Australia.

The remainder of this paper is organised as follows. Section 2 discusses key related work. Section 3 introduces the proposed approach, discusses the method by which the K-factor for a given environment is estimated, and details the algorithm used to collect the required multi-path data. Section 4 describes a set of experiments conducted in two urban sites in Wollongong and Sydney, New South Wales, Australia, in which channel measurements were taken to investigate K-factor behaviour. Section 5 describes the corresponding simulation, to which experimental results will be compared. Section 6 presents the results of both simulation and experimental measurements and evaluates the accuracy of the simulations. Section 7 discusses the significance of the key findings in this work, and makes recommendation for the use of the model.

2. Related Work

An early proposal for quantifying environmental dependence of channels was put forward by Aulin in [10]. The specular component was defined as the sum of squares of in-phase and quadrature components. These components were then defined as time-varying functions of Doppler shift and phase offset of the specular

signal. These parameters are influenced by the local environment and may be quantified in simulation. However, a method of approximating variations in the diffuse signal power remained elusive.

A study of the CDMA channel in forested areas was presented in [11]. It concluded that the Rayleigh-based modelling commonly used to predict the performance of CDMA base stations leads to overestimation of channel attenuation. If the Rayleigh assumption is used to set transmitter power levels, the overestimate of attenuation results in excessive levels of inter-cell interference. The authors show how the channel is better modelled as Rician, with a variable K-factor. While the work was primarily focused on influence of vegetation surrounding wireless transmitters on channel behaviour, the authors identified the importance of considering the effects of engineered structures (such as buildings). The authors primarily attribute the difficulty in finding a direct correlation between K-factor and vegetation density to the influence of anthropogenic environmental factors, demonstrating the need to consider surrounding building geometry in modelling of non-stationary fading.

In order to show the invalidity of the WSSUS assumption in VANETs, [3] uses two metrics, spectral divergence and coherence bandwidth, to analyse the channel in both the time and frequency domains. While the VANET channel was shown to violate the WSSUS assumption, the authors discovered there are so called *regions of stationarity*: areas in both time and frequency domains where the channel is locally WSSUS. However, it is noted in [4] that these regions of stationarity, while within the frequency range of 802.11p, may not last as long as the typical duration of a transmitted data frame. Acknowledging this problem, the authors of [12] present an optimised parameterisation of a local scattering function. They developed an estimator of the scattering behaviour of the environments in which they conducted their measurements, and then configured the parameters of the function based on channel measurements made in those areas.

Experimental measurements have since been used to model the behaviour of the K-factor. The first attempt to develop an analytic approach to K-factor modelling was published by Messier et al. in 2009 [9]. The authors conducted a wireless communication survey in a dense urban area in Canada, applying a moment-based K estimator from [5]. By analysing the statistical distribution of the K-factor measurements, they produced a Gaussian-based stochastic approximator for the K-factor that can be used in simulation. This provided a statistically accurate model of K-factor dynamics.

A similar approach was presented in [7, 8]. The authors used the results of the measurement campaign from [3, 4] and analysed the K-factor dynamics of the experiments, finding the parameter to vary in time, frequency, and space. They also found that the K-factor is dependent upon elements of the surrounding environment, such as the presence of scatterers and reflectors. The authors make an additional contribution in [8], in which they configure the parameters of a bi-modal Gaussian distribution to generate K-factors with the same statistical properties as those derived from their experiments.

A drawback of these stochastic models is that they are only useful for simulating the particular site of the original measurement campaign. A new set of channel measurements must be taken for any area

an investigator wishes to simulate, which can be impractical for large cities. An additional limitation is that while simulations based on this model may give accurate mean results for the entire area in which the original measurements were taken, due to its statistical nature, it may be inaccurate for a specific location within that environment.

An alternative approach to channel modelling is applied in [13]. The authors propose a geometry-based stochastic channel model (GSCM) to compute the channel impulse response based on the distribution of mobile (i.e. vehicles) and stationary (i.e. roadside trees and lamps) scatterers, and verified the model using a channel measurement campaign in Lund, Sweden. In the model, the scatterers were randomly distributed between lanes of a highway and along it's length. This work also discusses the possibility of using vehicular mobility models (e.g. SUMO [14]) in the computation.

This methodology was extended in [15]. As in [13], the authors stress the use of simplified ray-tracing approaches through 2D representations of the simulation environment to parameterise the channel impulse response. The complete parameterisation of the model is presented for various environments (e.g. campus roads and highways) for use in V2V scenarios, along with verification of the proposed model compared with GSCM. These models are of particular interest, as they show that the VANET channel may be modelled using simplified geometric components.

3. *K*-factor Approximator

By analysing the signal paths intercepted by the receiver, the K-factor for that source-destination channel may be approximated. Knowledge of the environment - in particular, building geometry, placement, and composition - is required to determine the multi-path components necessary for the approximation.

3.1. K-factor Approximation Method

Power radiated from an omnidirectional antenna is quantised (in two dimensions) into N_{ray} rays, each having an initial power level of

$$P_{ray} = \frac{P_{TX} G_{TX}}{N_{ray}} \tag{2}$$

where P_{TX} is the total transmission power of the wireless device, and G_{TX} is the gain of the device's antenna.

The quantised rays are radiated in all directions from the transmitter. A ray is determined to have been intercepted by the receiver if it passes through the effective aperture of its antenna. The effective aperture is given by

$$A_e = \frac{G_{RX} \lambda^2}{4\pi} \tag{3}$$

The power contribution of the i'th received ray is determined by the number of reflections it has undergone, N_i^{ref}, and the reflection coefficient Γ of each reflective surface. Γ is dependent on the relative

permittivity of the surface material ε_R and the incident angle θ_I:

$$\Gamma = \frac{\sqrt{\varepsilon_R - \cos^2\theta_I} - \varepsilon_R \sin\theta_I}{\sqrt{\varepsilon_R - \cos^2\theta_I} + \varepsilon_R \sin\theta_I} \tag{4}$$

Consecutive reflections are modelled by multiplying their reflection coefficients, such that the combined coefficient of the i'th ray is

$$\Gamma_i^T = \prod_{n=0}^{N_i^{ref}} (\Gamma_n)_i \tag{5}$$

and the power of the ith ray is [1]

$$P_i = P_{ray} \left(\Gamma_i^T\right)^2 \tag{6}$$

The receiver forms a set Q of rays that pass through its aperture after reflecting through the environment. The specular and diffuse ray sets are then $Q_S = \{i \in Q | N_i^{ref} = 0\}$ and $Q_D = Q \setminus Q_S$. The K-factor can now be estimated by

$$\hat{K} = \frac{\sum_{i \in Q_S} P_i}{\sum_{j \in Q_D} P_j} \tag{7}$$

(7) has the useful property of being scale-invariant. That is, it is independent of the transmitter power or gain. By substituting (6) into (7):

$$\hat{K} = \frac{\cancel{P_{ray}} \sum_{i \in Q_S} \Gamma_i}{\cancel{P_{ray}} \sum_{j \in Q_D} \Gamma_j} \tag{8}$$

Thus, the approximator is purely a function of the communication environment. This was predicted by Messier et al in [9]. It should be noted that the formula is not independent of the *receiver* properties, in particular, it depends on the effective aperture of the receiver.

3.2. Ray-launching Algorithm

As a proof-of-concept, a simple geometric intersection algorithm was used to trace rays through a top-down view of the building environment, with the faces of each structure tagged with the permittivity of the material from which that structure is composed. The model is purely two dimensional; it is assumed that there are no overhead reflectors - meaning that any signal power directed skyward can be considered lost (a similar approach to models proposed in [13, 15]). Considering only a two-dimensional plane simplifies the modelling of K-factor while simplifying construction of the simulation scenario and minimising computational complexity.

The ray-launching approach allows for multiple receivers to determine the K-factor for specific channel to the transmitter using a single execution of the algorithm, shown in Figure 1. The initial length of each

[1] The approximator was first published in IEEE ICC 2014 [16]. There was an error in the derivation that influenced the results published in the paper. The error has been fixed and better results have been obtained. The authors would like to thank the reviewers of Physical Communications Journal for recognising the error and pursuing the matter.

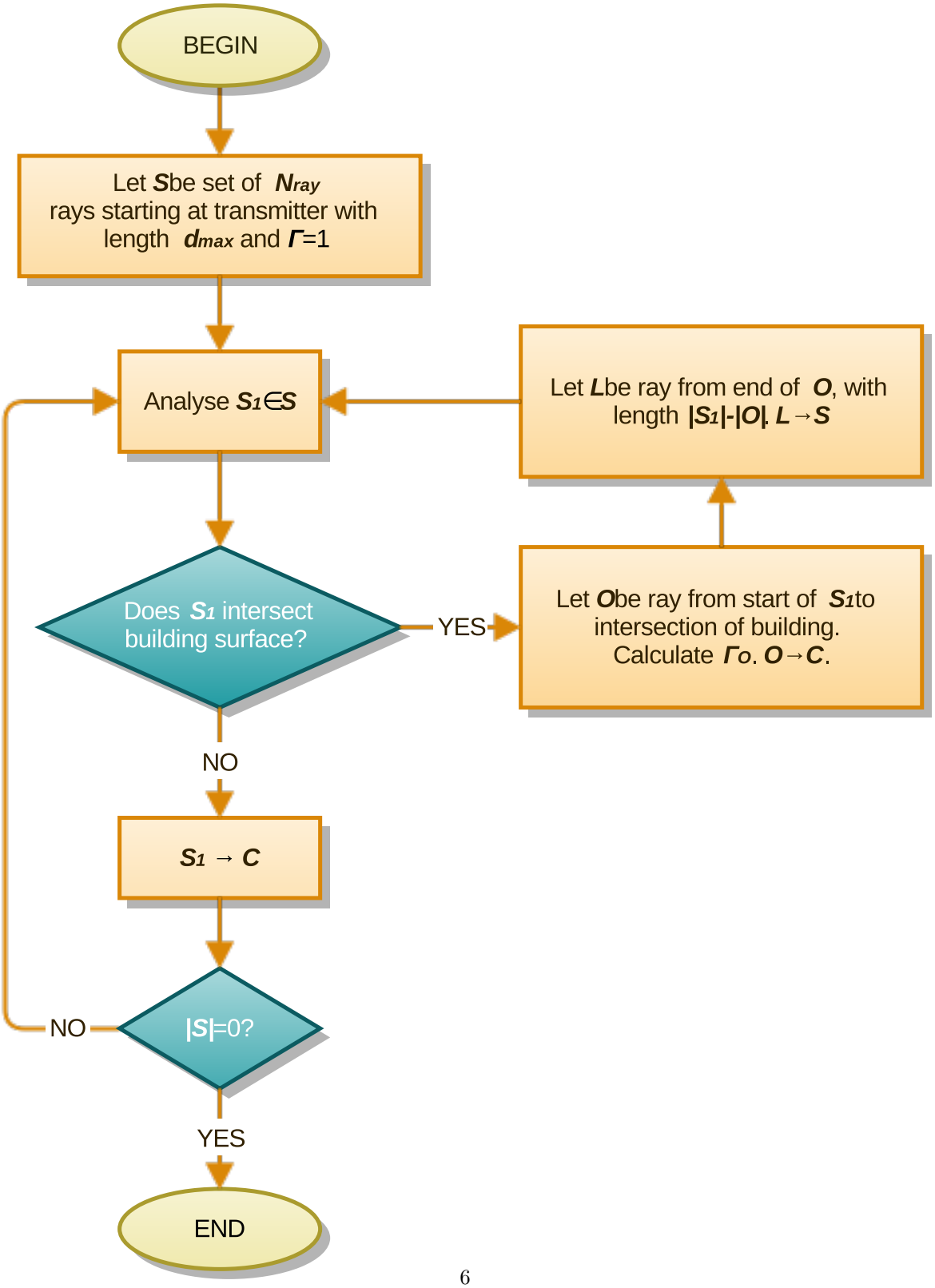

Figure 1: The ray-launching algorithm.

ray, d_{max}, is determined by the free-space pathloss model as

$$d_{max} = \sqrt{\frac{P_{TX} G_{TX} A_e}{4\pi S}} \tag{9}$$

where S is the sensitivity of the receiver. This criterion introduces a dependence of the approximated K-factor on transmission power. However, this dependence does not affect the magnitude of the result, but rather the maximum distance over which approximation is valid. When a reflection occurs, the new ray's coefficient is computed from (4), and it's length is given by

$$\Delta d = \Gamma d_{max} - d \tag{10}$$

Once the algorithm has computed the ray distribution for the given number of rays initially launched from the transmitter, each receiver can simply use its location and effective aperture size to calculate the number and power of rays (out of the total launched) reaching the aperture, and hence obtain the total power received at that location. The resultant set of ray paths are used to determine the K-factor as per (7).

3.2.1. Performance Considerations

A multithreaded implementation of the algorithm has a worst-case execution time of the order of

$$\mathcal{O}\left(\frac{N_{ray}^2 \rho_B \pi d_{max}^2 \mu_E}{N_{core}}\right) \tag{11}$$

where ρ_B is the density of buildings per unit area, μ_E is the average number of edges per building, and N_{core} is the number of cores used in the simulation. Typical execution time for the ray-launcher is explored in Section 5.

3.2.2. Building Geometry Data

At present, this model does not take vehicles into account; only static building geometry is considered. The building data is taken from Open Street Maps (OSM) [17]. It is straightforward to add additional attributes to the XML descriptors of building definitions provided by Open Street Maps, including the material out of which each building is predominantly composed. The validity of this method has previously been established in [18]; the authors found the approach provided results in close agreement with those obtained by applying building data supplied by local government, especially in verifying channel sounder measurements with raytracing simulations [19].

3.2.3. Permittivity of Building Materials

The permittivity of several common building materials at 2.41 GHz is listed in Table 1. These parameters are used throughout the simulations.

Material	ε_r	Reference
Glass	2.3	[20]
Stone	4.5	
Concrete	5.4	
Concrete (non-reinforced)	8.721	[21]
Polycarbonate	2.86	
Gypsum	2.518	
Brick Wall	3.743	

Table 1: Relative Permittivity of various common building materials [20, 21].

4. Experimental Work

A set of experiments was carried out in order to obtain measurement of K-factor and PDR in live traffic situations. The approximation method presented in Section 3 was verified by comparison of its K-factor estimates with the results of these experiments. The methodology applied here will also be adopted for the simulation.

The experiments were conducted in local urban and industrial areas of Wollongong and Sydney, NSW. These areas were selected based on their accessibility, the type and number of buildings in the area, and whether there were times at which vehicle density was very low. Two sites were chosen: Kingsway Road (Figure 2) in Miranda, a southern suburb of Sydney; and Burelli Street (Figure 3) in Wollongong.

Burelli Street is a long, straight stretch of four-lane road punctuated by multiple intersections. It is frequented by heavy traffic during daylight hours and is virtually deserted at night, providing a site where the channel can be analysed in the presence and absence of vehicles in LOS conditions. The site in Miranda is a built-up urban block, with one street being a part of a freeway and the others bordering residential apartments. The presence of Non-Line-Of-Sight (NLOS) areas allows K-factor comparisons with the LOS areas of Burelli street.

The Burelli Street experiments were conducted in the presence (10:00 AM - 12:00 PM) and absence of vehicles (11:00 PM - 1:00 AM) during May 2012. The maximum speed limit on Burelli Street is 50 km/h. Miranda experiments were conducted only in the absence of vehicles, between the hours of 11:00 PM and 5:30 AM, also during May 2012.

4.1. Experimental Apparatus

Two wireless testing platforms were used, each consisting of the following:

- PCEngines Alix 3d3 systems running Voyage Linux 0.8

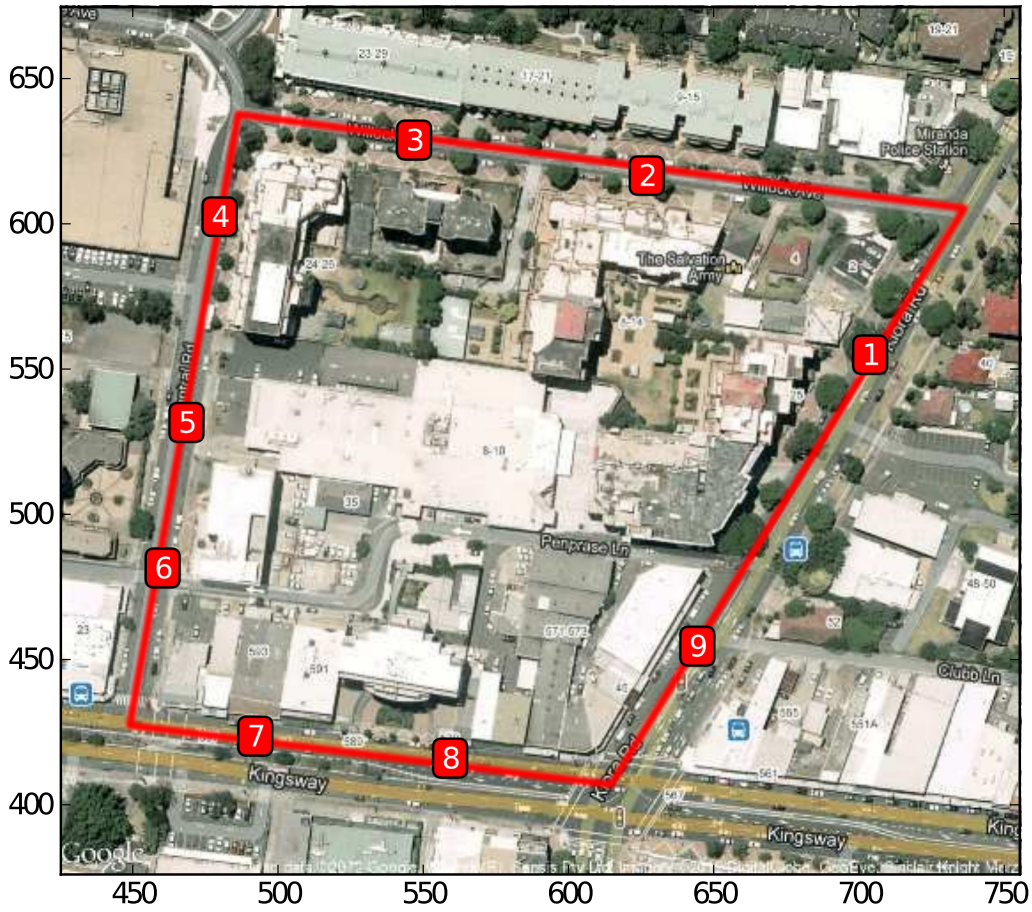

Figure 2: Satellite map of the Miranda experiment site. The red line indicates the path travelled by the mobile transmitter; the numbers on the path indicate the position of the receiver at each stage of the experiments.

Figure 3: Satellite map of Burelli Street, NSW. The location of the receiver, path of the transmitter (cyan), intersections (green) and point of maximum range (red) are indicated.

- Ubiquiti SR-2 400mW 802.11b/g cards (ath5k drivers)
- Generic 5dBi gain omni-directional antennas
- System coordination and data logging laptop

One platform served as a stationary receiver; the other was a mobile transmitter, which travelled along the route indicated by Figures 2 and 3, transmitting CBR bursts of 100 500-byte packets three times per second. The average data rate was 1.2 Mb/s with a carrier frequency of 2.412 GHz and a physical data rate of 11 Mb/s. This channel was selected for minimal interference from existing wireless networks following a brief survey. The receiver was additionally equipped with a Rohde and Schwarz FSH8 spectrum analyser which sampled signal spectra during as the packet burst transmissions. Packets additionally contained the GPS location of the transmitter, which were recorded together with signal power and Packet Delivery Ratio (PDR) measurements for each burst. Data was collected as the transmitter made ten circuits, at a constant speed of 20 km/h.

Transmitter positions were quantised to ten metre increments over the total length of the test path. Signal measurements were then collated at each of these transmitter positions, from which K-factor values were extracted. PDR measurements were collated for MAC layer performance comparison.

4.2. Estimation from Experimental Data

While the most accurate method of K-factor estimation would be a best-fit curve matching of the Signal Power CDF, this method was difficult to reliably automate. There exist a number of alternative moment-based methods in the literature. Of these methods, the estimator proposed by Greenstein was most easily applied to the data collected from experiment [22]. Greenstein's estimator is given by

$$\hat{K}(n) = \frac{V(n)}{G_a(n) - V(n)} \tag{12}$$

where

$$\begin{aligned} G_a(n) &= \frac{1}{N_W}(|c(n)|) * w(n) \\ G_v^2(n) &= \frac{1}{N_W} \sum_{i=-\infty}^{\infty} \left[w(i) \left(|c(n-i)| - G_a(n) \right)^2 \right] \\ V(n) &= \sqrt{G_a^2(n) - G_v^2(n)} \end{aligned}$$

and where $c(n)$ is the vector of channel samples and $w(n)$ is a rectangular window of width N_W.

The accuracy of the estimation depends on the value of N_W. In the experiment, it was difficult to ensure that each transmitter position received the same number of channel samples for consistent accuracy. Thus, the analysis required a minimum number of channel samples to ensure the computed K-factor would accurately represent the dynamics of the data collected.

A simple procedure was used to determine an appropriate minimum number of samples for satisfactory statistical significance. A fading waveform of known K-factor, K_n was firstly generated according to

$$c\left(n\right) = G_f\left(n, K\right) = \frac{\left(X_1\left(n\right) + \sqrt{2K}\right)^2 + X_2^2\left(n\right)}{2K+1} \tag{13}$$

where X_1 and X_2 are independent Gaussian random variables with zero mean. This is based on Jakes' model for Rayleigh fading, which has been used previously in this research project [23]. The error between the estimate and the true value of the K-factor, $E_k = \left|\hat{K} - K_n\right|$ was then computed for increasing values of N_W. Figure 4 shows that the error between $\hat{K}$ and K_n decreases exponentially with increased N_W. Based on curve this, a minimum sample size of 30 is selected for analysis, as the residual error is small, but N_W is not impractically large (from an experimental and simulation perspective). Any transmitter positions with fewer than 30 samples were therefore excluded from analysis.

5. Simulation

The K-factor approximator and necessary support classes to load the building edges from the OSM maps were integrated into the OMNeT++ Network Simulator [24]. This is a widely used simulator which can be

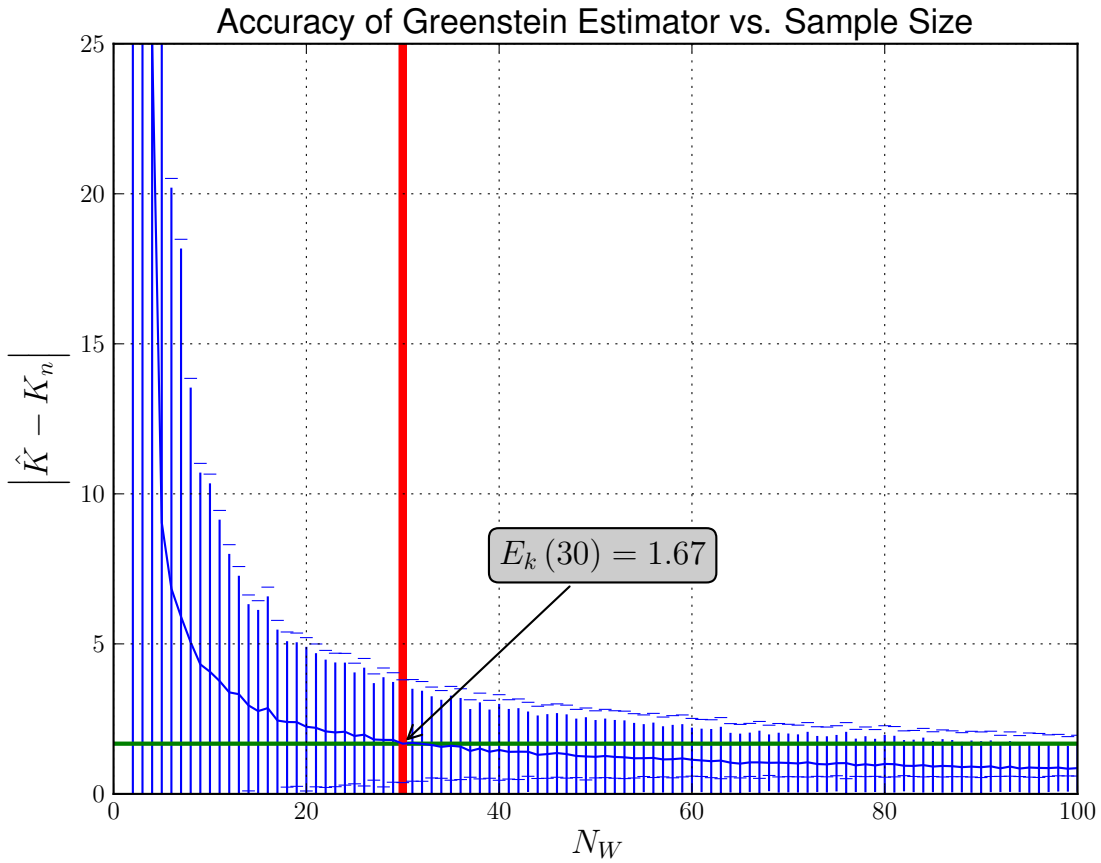

Figure 4: The error of the K-factor estimator decreases exponentially with increasing sample size. Error bars represent one standard deviation. At approximately $N_W = 30$, the error is considered acceptably small for the purpose of this work.

coupled to the SUMO traffic simulator [14] through the VEINS API [25].

Both simulated nodes use the MiXiM implementation of the 802.11 MAC and PHY layers, without a network layer (as it is not relevant for this study). All packets were broadcast, removing the necessity for routing and association. Packets were sent at a static 11 Mb/s at 2.412 GHz, with the same parameters as used in the experiment (three bursts of 100 500-byte packets transmitted per second).

The approximated K-factor was not recorded in the results. Instead, for consistency with the experimental results, power measurements logged by the receiver were used to calculate the sample K-factor using the same analysis techniques as in Section 4.

The CORNER pathloss model was applied [23, 26–28]. Equation 13 used the output of the K-factor approximator to compute the fading gain. The resultant received signal power is then given by

$$P_{RX} = P_{TX} G_{PL} G_f \tag{14}$$

6. Results

Note that in all results, K-factors are expressed as a simple power ratio (i.e. not in decibels).

6.1. Behaviour in LOS

In Figure 5, the K-factor follows an upward trend with increasing distance, until approximately half-way down the street, at which point it begins to decrease. When the transmitter and receiver are close to each other, with reflectors nearby, the resultant diffuse paths have similar lengths and there are fewer reflections; thus they will interfere with the specular path, reducing the K-factor. As the transmitter moves further from the receiver, the diffuse paths tend to reflect more and travel further, and thus diminish to a greater degree, allowing the specular path to remain dominant. This is analogous to viewing a point light source in a dark room. When near the source, a person can easily see objects illuminated by the reflected light. However, when viewing the source from a greater distance, reflected light becomes progressively dimmer while the point source itself remains strongly visible. Thus at greater distances, path-loss effects dominate the specular path, and the K-factor falls.

The normalised autocorrelation of the K-factor against distance was computed for the simulation with 1024, 2048, and 4096 rays as well as the experimental data. These curves are shown in Figure 6. The approximator performance converges to the experimental results as the number of rays increases, as expected.

Figure 7 shows a plot of PDR versus distance. The plots show a close agreement between the experimentally measured PDR in the simulation results over the first 100 metres (beyond 100 metres, connectivity is intermittent and so an accurate PDR estimate is difficult to obtain). Increasing the ray count beyond 1024 rays appears to provide little improvement in this case. Furthermore, the mean experimental PDR is

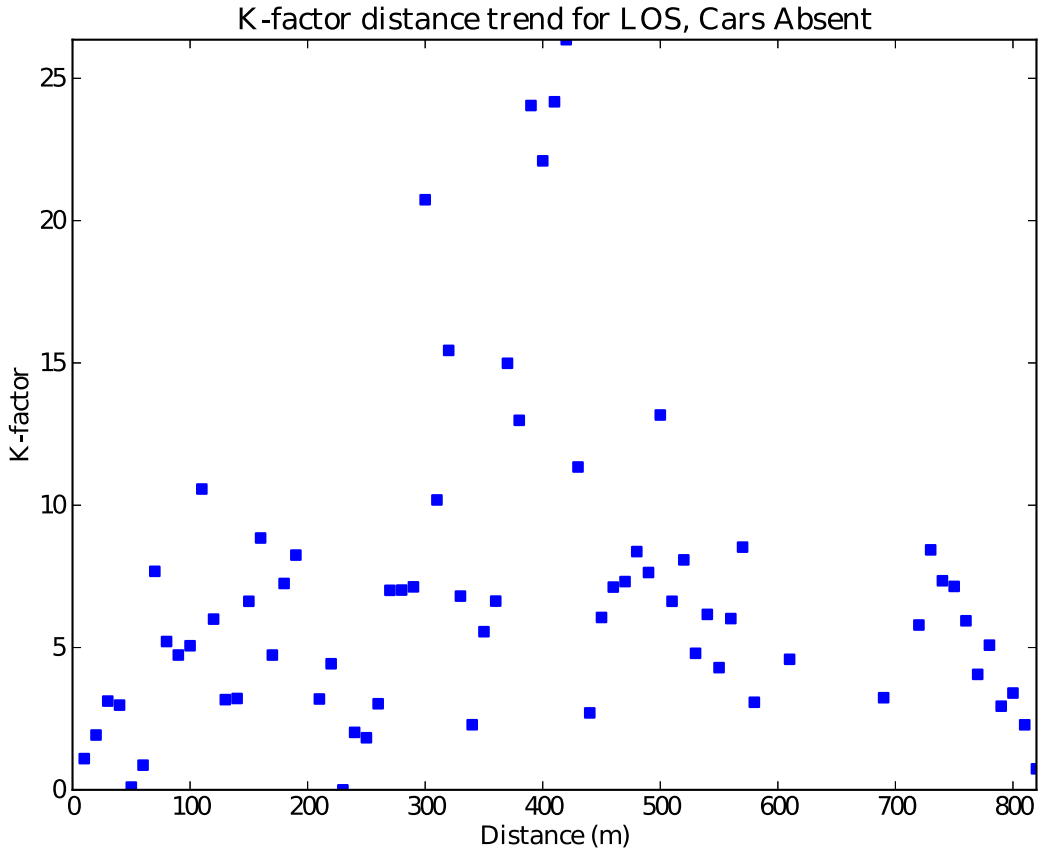

Figure 5: K-factor versus distance on Burelli Street.

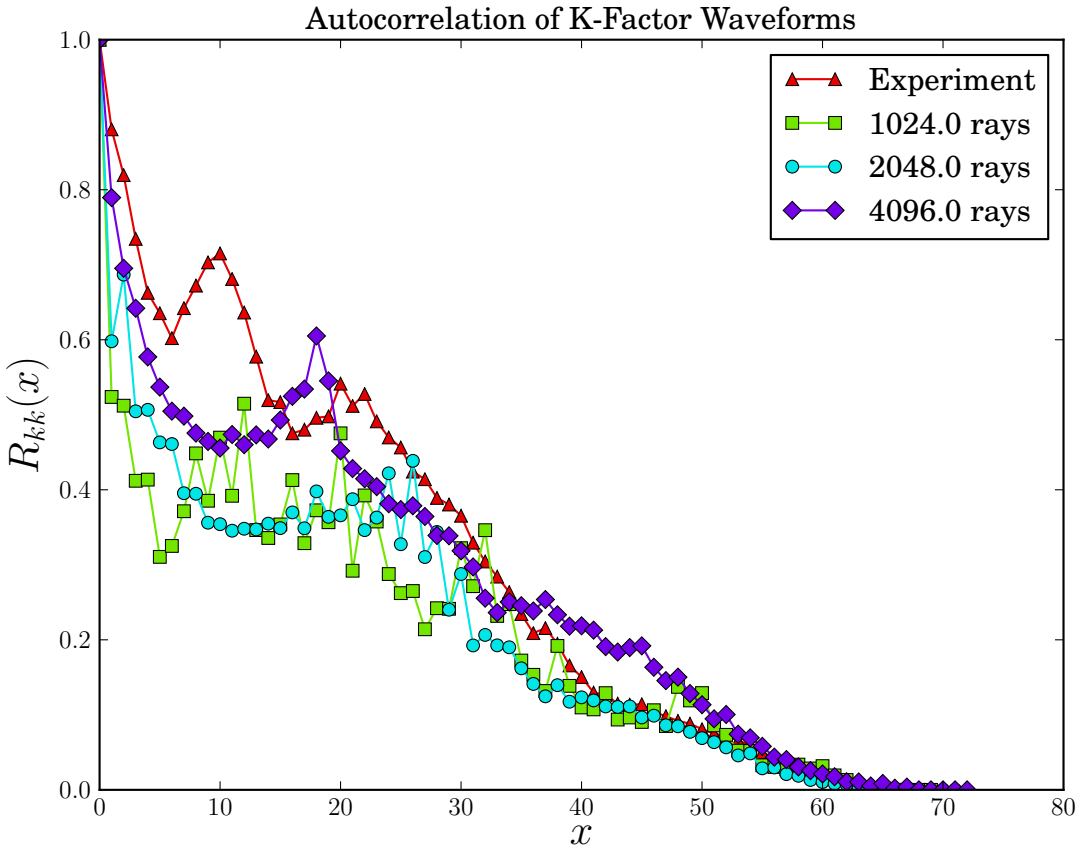

Figure 6: Autocorrelation of K-factor for experimental results and simulations with 1024, 2048 and 4096 rays.

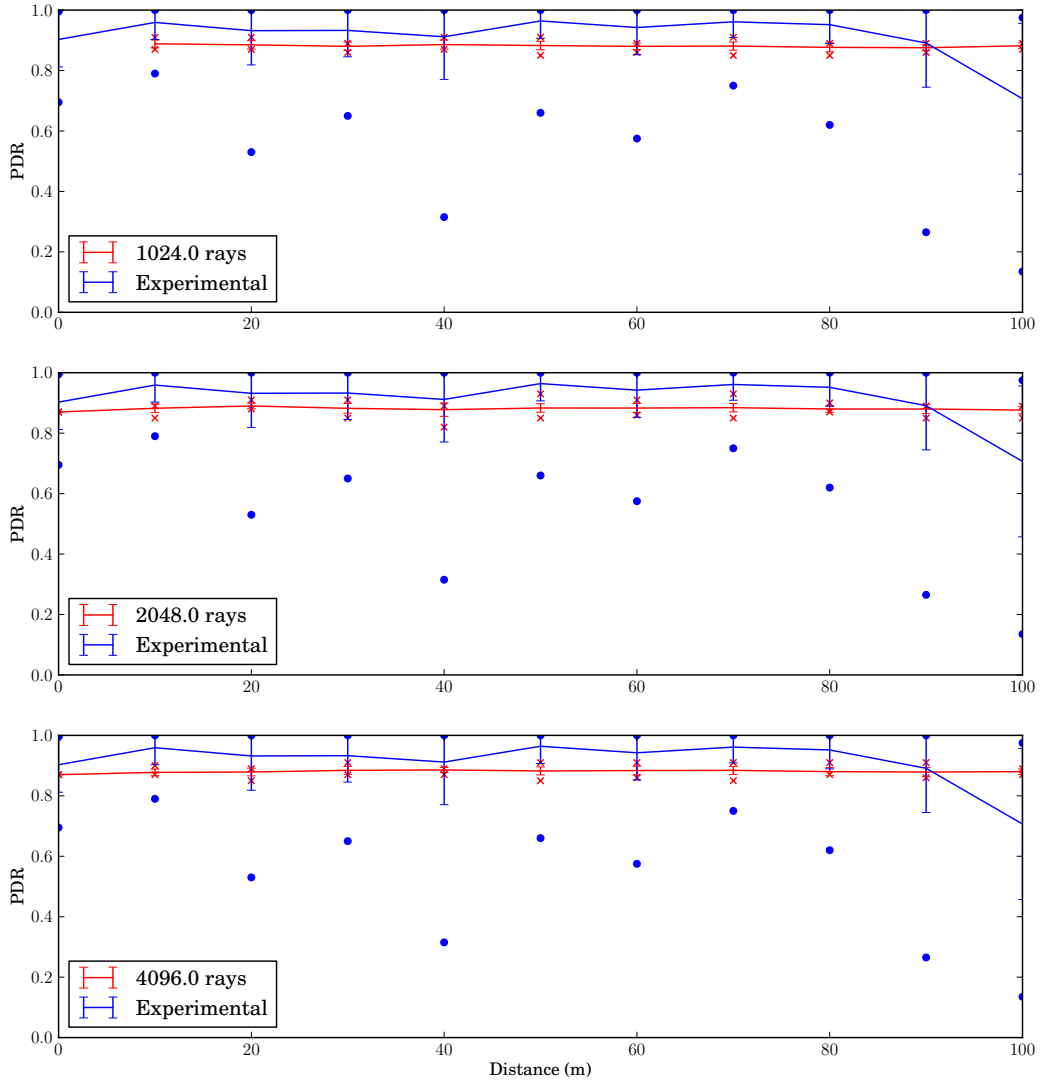

Figure 7: PDR behaviour over a range of 100 metres for three 1024, 2048 and 4096-ray simulations in the absence of vehicles. The error bars represent two standard deviations, and the coloured markers indicate maxima and minima.

higher than the simulation. The discrepancy between experiment and simulation may be attributed to an observed pseudo-waveguide effect caused by building walls [28], which may boost received signal power and thus PDR. Since the simulation does not attempt to account for this effect in the pathloss calculations, the mean PDR is slightly lower than observed in the experiment.

Despite these discrepancies, there is agreement between experiment and simulation over short range. As mentioned in [29], a transmission range of 100 metres is sufficient for most VANET applications. This is an important result in the application of this K-factor model to the validation of certain VANET scenarios, such as clustering, RSU association, and vehicular collision warning systems.

6.2. Approximator Issues

While in LOS, the proposed system provides a good representation of the experimental K-factor. However, the experiment data reveals certain issues with the approximator in terms of vegetation and NLOS scenarios.

6.2.1. Behaviour in NLOS

Initial analysis of K-factor distribution plots for Miranda, shown in Figure 8, revealed that experimental K-factors tend to be higher in NLOS than in LOS at shorter ranges. In the NLOS case, even though there is no direct path, some signal power is diffracted around building corners; it seems that these refracted signals remain dominant over reflected paths, resulting in a higher K-factor in the NLOS case.

Figure 9 shows that in the NLOS case, the K-factor can be up to four times greater than the corresponding values in the LOS case. Figure 9d shows a sudden increase in K-Factor values beyond approximately 120 metres. This matches with the four readings after the turn into Penprase Lane in the corresponding satellite image, suggesting that significant power is lost through diffuse rays which escape via intersecting side-streets. Additionally, these areas have significant numbers of road-side trees and other foliage, which can act as an absorbent or scattering medium.

These results indicate a current drawback of the approximator presented in Section 3. Specular rays having undergone no reflections are required for a non-zero K-factor, meaning that NLOS scenarios would result in Rayleigh fading. However, the results show the possibility for the K-factor to be non-zero in NLOS. In future work, the approximator may need to be modified to incorporate diffraction effects that lead to non-zero K-factors when the source and destination are not in direct line of sight.

6.2.2. Vegetation

The results of the experiment and corresponding simulations are included in Figure 9. The results shown are for the simulation performed with 1024 rays. There is very limited agreement between simulation and experiment for locations 2 and 3. The local environment at these positions includes both significant

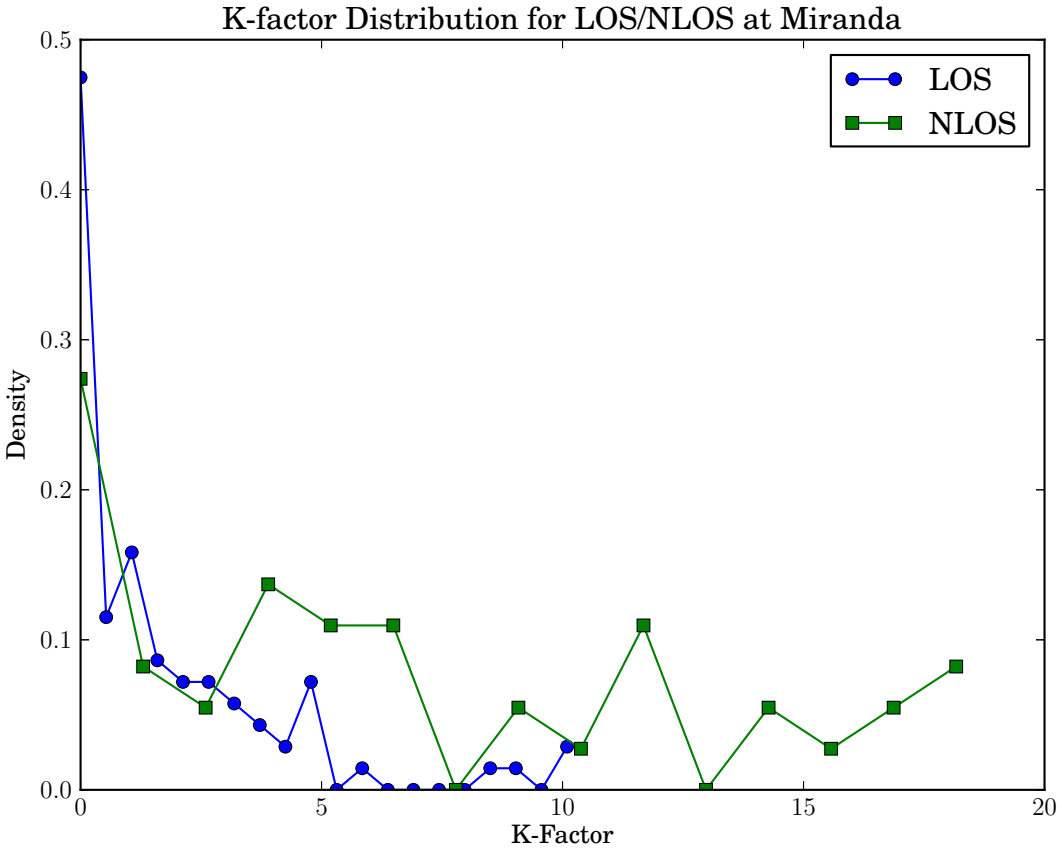

Figure 8: K-factor distribution in LOS and NLOS cases.

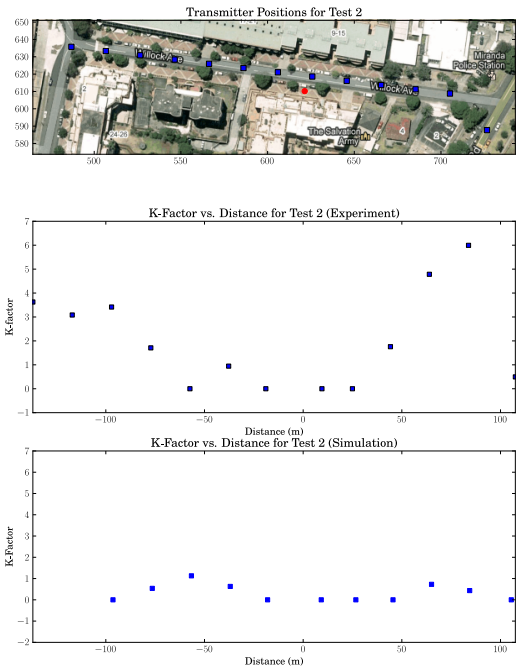

(a) Location 2

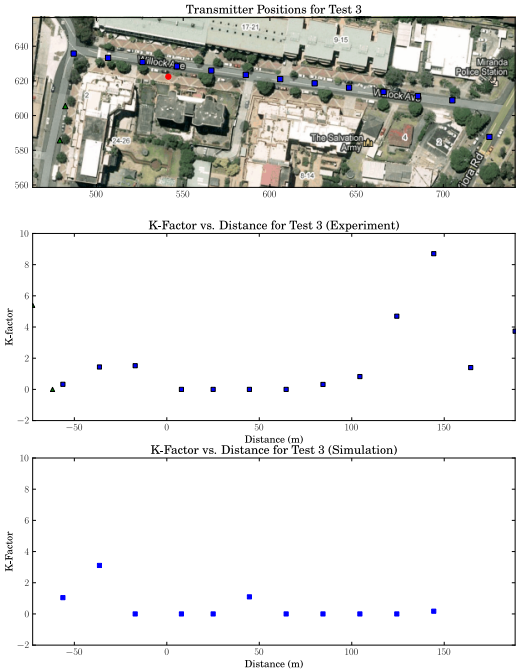

(b) Location 3

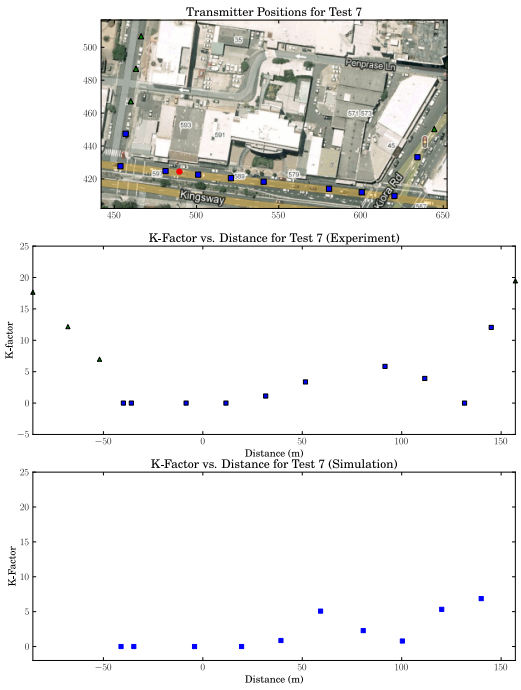

(c) Location 7

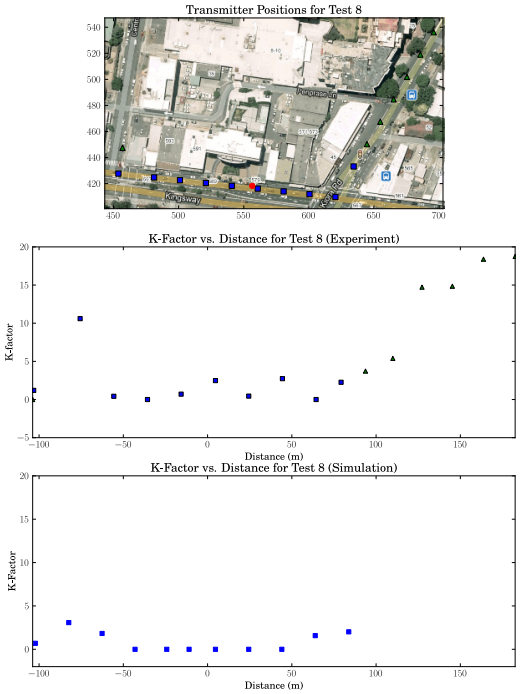

(d) Location 8

Figure 9: K-Factor versus distance for four separate scenarios. The red dots indicate the position of the receiver. The gaps in the lower scatter plots correspond to points where the simulation K-factor reached values higher than observed during the experiment.

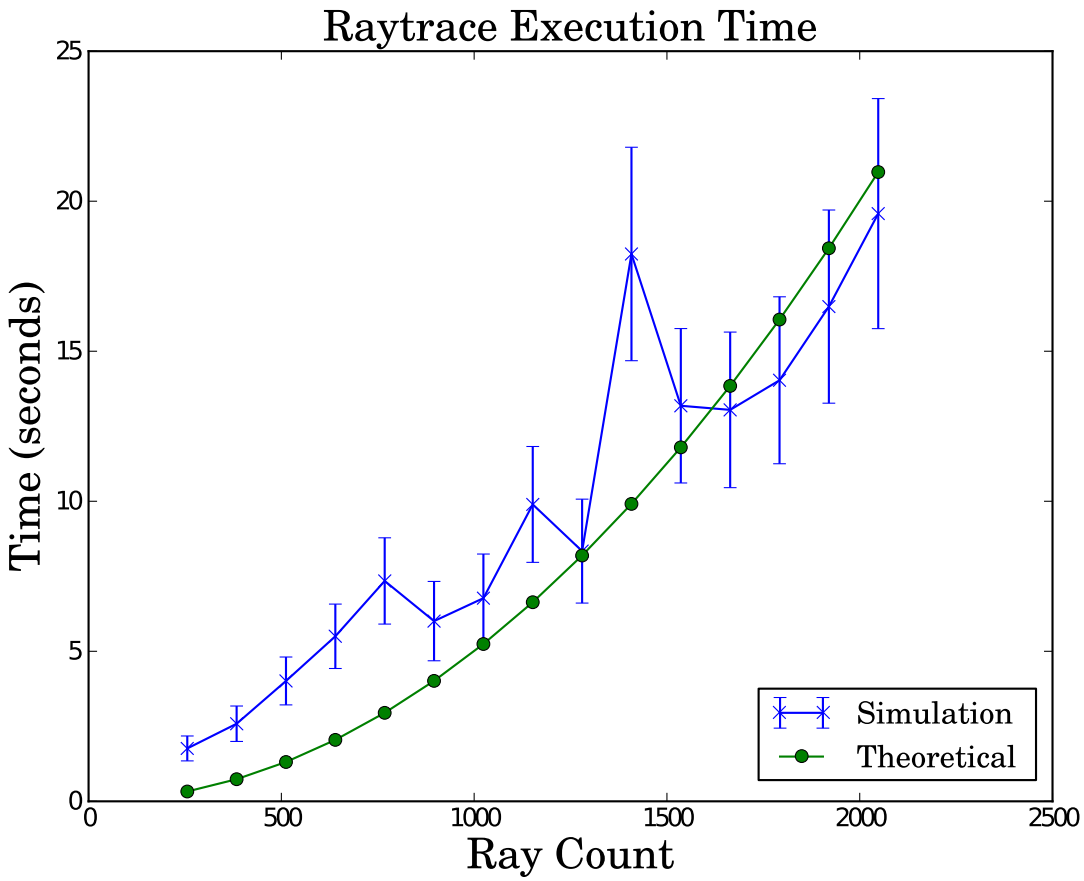

Figure 10: Comparison between actual simulation time and analytic estimate of simulation time. One significant outlier is observed for 1408 rays.

amounts of vegetation as well as other vehicles, which the model does not yet take into account. The graphs for locations 7 and 8, which included much less vegetation, show a closer agreement between experiment and simulation.

The experiment results indicate that vegetation is absorbing signal power, which prevents it from reflecting off buildings and other objects. As a result, less diffuse power is reaching the destination and the K-factor is thus higher. Future work will entail further experiment to determine the extent of absorption to adequately account for the presence of vegetation in K-factor approximation.

6.3. Computational Complexity

The simulation recorded the time taken for each pass of the path resolver at different ray counts, and the results compared with the predicted time complexity given in Section 3.2, shown in Figure 10.

The simulations broadly followed the predicted execution time. It should be noted that in the simulation,

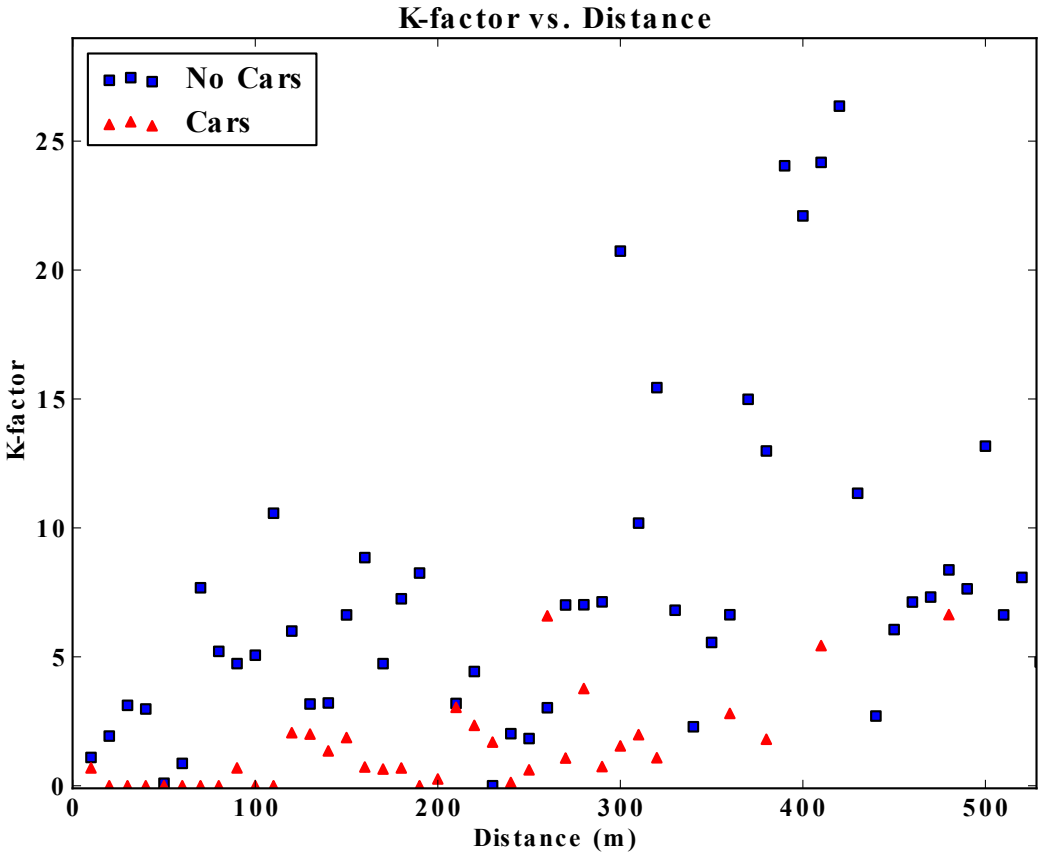

Figure 11: Plot of experimental K-factor in the presence and absence of vehicles.

only one car was transmitting with no acknowledgement frames being exchanged. In a full VANET simulation, in which hundreds of vehicles are present and transmitting regularly, execution times make simulation computationally infeasible.

Due to the static nature of buildings, the ray-launcher may be moved into a pre-simulation step. During the preparation of the road network from OSM data, a separate program may calculate and store K-factors for pairs of transmitter and receiver positions to be indexed in simulation. In so doing, the ray-launcher need only be run once, and the file retained along with the rest of the road and traffic load data.

6.4. Vehicle Considerations

Experiments were also conducted on Burelli Street during the day, when vehicles were present, and the results compared to simulation. Figure 11 indicates the most direct effect of the presence of vehicles is a significant reduction of the K-factor. The low K-factor suggested a Rayleigh fading channel in this area; however, additional simulations with $K = 0$ do not support this conclusion, as seen with the PDR plot in

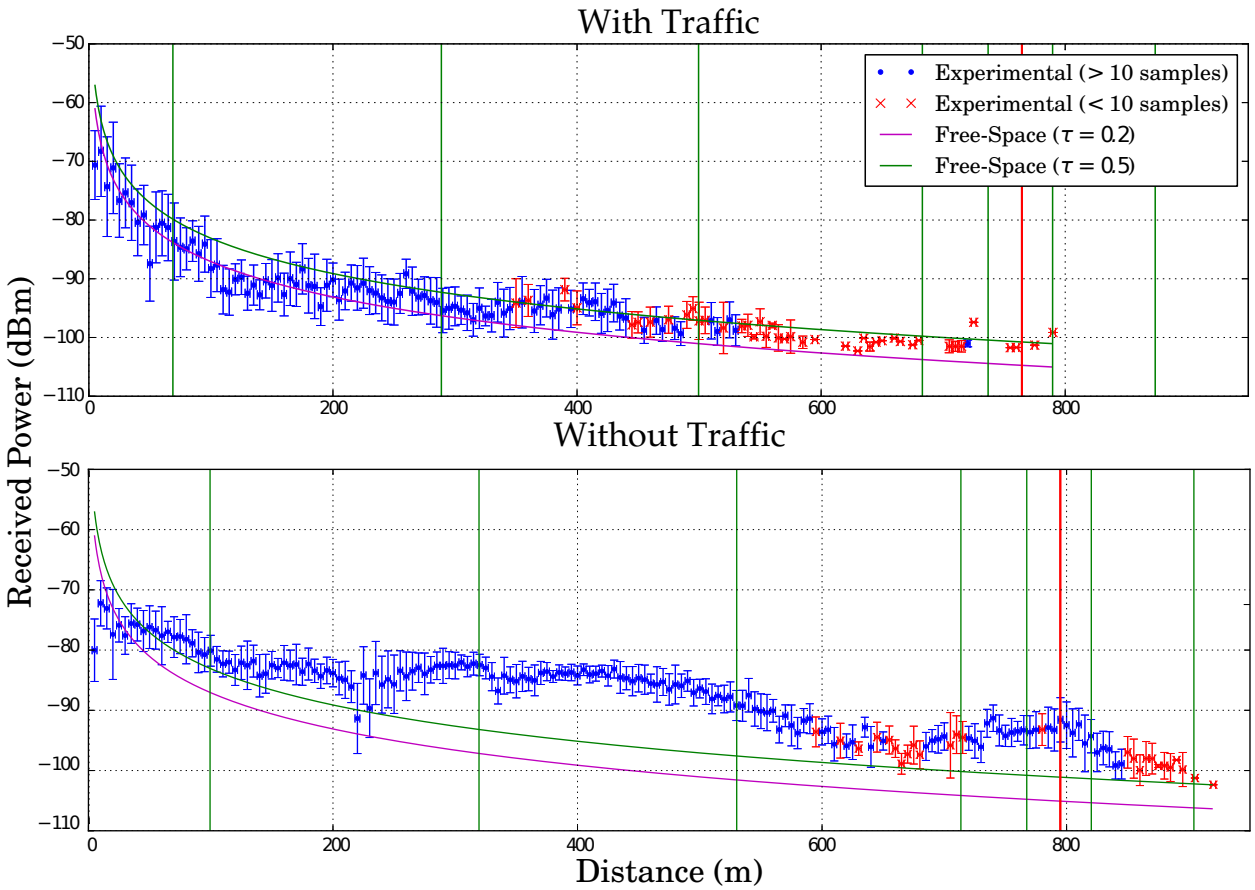

Figure 12: Power measurements taken on Burelli Street, with and without vehicles. τ is an experimentally derived constant [28].

Figure 13.

The plots of signal power shown in Figure 12 suggest that, in the absence of vehicles, the waveguide effect observed at Burelli causes a significant boost in signal power. This presence of vehicles negates this boost, suggesting that vehicles block or scatter signal power that reflects from roads and building walls.

Shadowing effects typically exhibit a log-normal distribution [30, 31]. The combined attenuation due to shadowing and Rician fading then becomes log-normal-Rice distributed. The measurement campaign in [32] found that the parameters of the Rice and log-normal distributions were uncorrelated, meaning that the attenuation due to shadowing can be independently modelled using a separate approach. However, this introduces the need for an additional method to estimate the parameters of the log-normal distribution based on vehicle density in the LOS path. While the development of such an approximator is an objective of ongoing research in modelling scattering due to atmospheric turbulence [33], there is currently no known method of approximation for vehicular obstructions. Furthermore, experimental work on non-mobile vehicular obstructions show that, based on the proximity of communicating vehicles to large obstructions such

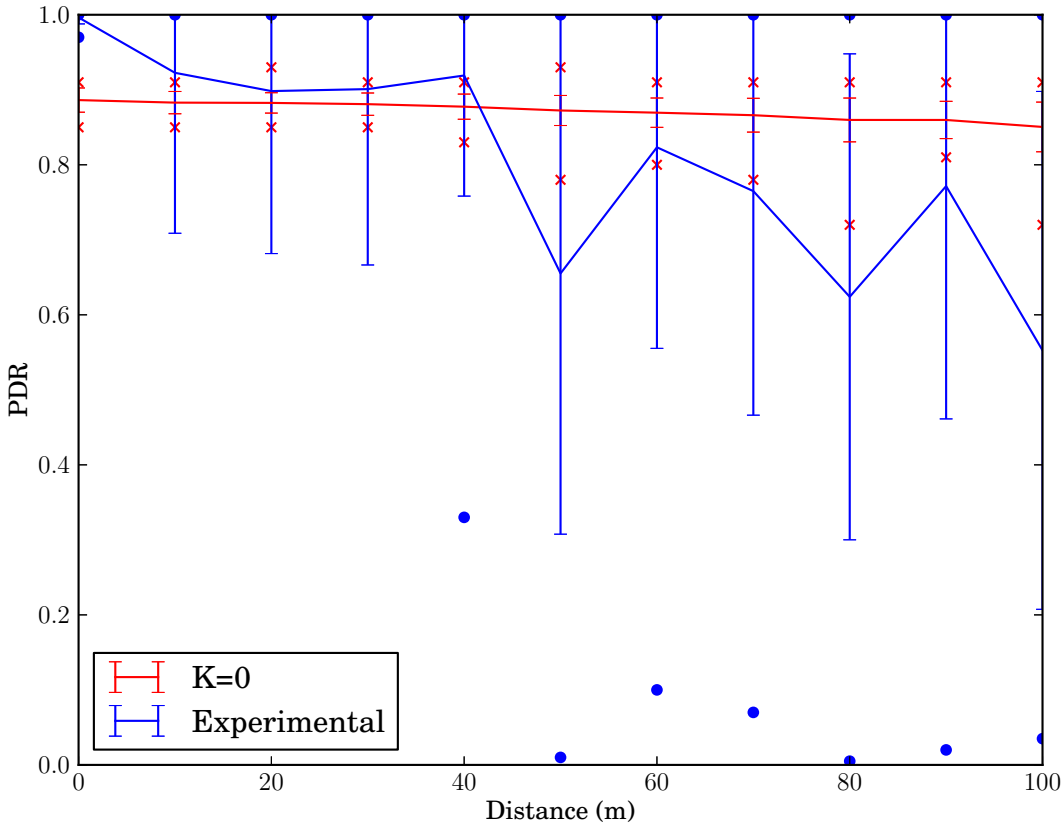

Figure 13: Simulated PDR behaviour over the first hundred metres with a Rayleigh fading model, compared with experimental PDR in the presence of vehicles.

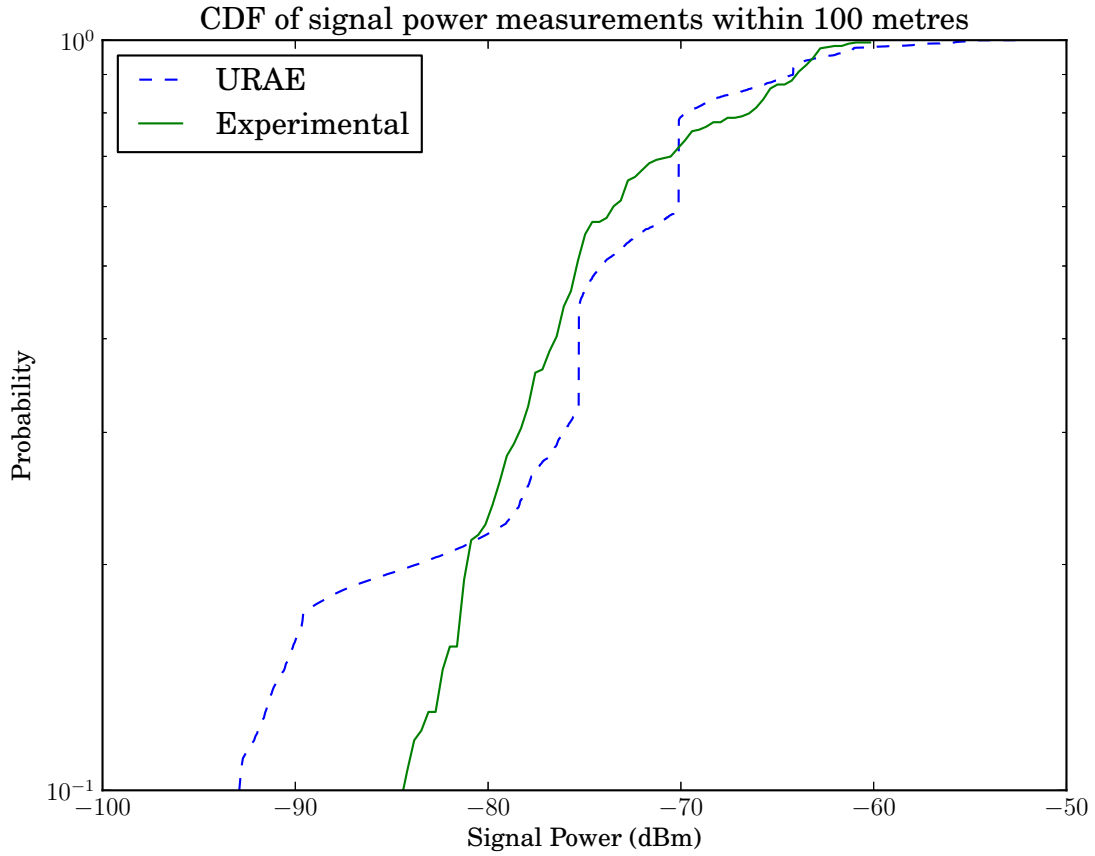

Figure 14: CDF of signal power within the first 100 metres.

as buses, the distribution is better described by Nakagami-M models [34]. On the other hand, deterministic models such as the knife-edge diffraction model have been implemented and are well-known, and appear to be sufficient to capture the transient nature of vehicular obstructions. Therefore, the deterministic method is preferable.

Further simulations were carried out using a three-ray knife-edge shadowing model as proposed by Wang et al. [35]. The authors had performed experimental verification on their model, and found good agreement between measurement and theory. This model was implemented in OMNeT++ and simulated on top of the K-factor approximator.

Figure 14 shows the CDF of received power within the first 100 metres. The plot shows a close agreement between experiment and simulation for the physical layer at close range, although the simulation tends toward lower signal power values. Figure 15 shows the trends in PDR against distance at close range. The presence of vehicles causes irregularity in the distribution of signal power and the corresponding sharp drops in PDR.

Figure 15: The addition of shadowing improves the accuracy of PDR estimates at the MAC layer.

7. Discussion and Conclusions

This work presented a method for generating a good approximation of the Rician K-factor through a simple ray-casting model of the propagation environment. Experiments have been performed in a vehicular environment, both in the presence and absence of vehicles, revealing certain properties of the K-factor with respect to the environment. Vegetation appears to exert a shadowing and absorption effect rather than scattering. A particularly interesting result is that intersections result in an increase in the magnitude of the K-factor, which appears to be a result of diffuse signal power escaping and becoming unavailable to the receiver. These experiments, in conjunction with simulation work, have verified the validity of the proposed the K-factor approximator.

The model will be particularly useful in improving the accuracy of simulations for short-range VANET applications, for example, in simulating clustering and RSU association. It is best suited to modelling built-up urban environments with minimal vegetation, such that the only environmental objects of great influence are buildings. The future addition of an appropriate vehicular shadowing model will make the proposed channel model very useful for accurate multi-vehicle VANET simulations. The principle bottleneck in such use is the prohibitively time-consuming ray-launching algorithm which would need to be repeated for each transmission. However, it is likely that further opportunities for optimisation still exist, which will reduce the necessary simulation time.

Other planned future work includes the incorporation of a wider range of phenomena to be considered in the approximation. This includes smaller static objects, such as lamp-posts which are more likely to scatter signal power than reflect it. Vegetation should also be considered in order to improve the approximator's applicability in a wider range of environments. The antenna's location and radiation pattern also should be considered, as well as V2I properties, since both will influence the behaviour of the VANET channel [36].

As the ray-launching algorithm was chosen purely to prove the concept of K-factor approximation via path resolution, another avenue of improvement is to research different methods of acquiring the necessary multipath data. Ray-tracing using graphics hardware has been extensively researched for modelling all elements of the channel [37–39]. Due to the much smaller scale objective of modelling K-factor dynamics, simplified approaches can be used to obtain multipath component data with faster execution times.

Acknowledgements

The authors would like to thank Steve Tree of Rohde & Schwarz, Australia, for providing the spectrum analyser hardware that made this experimental work possible, and Chris Cooper for serving as driver for the mobile transmitter unit. The voluntary input of the reviewers of Physical Communication Journal is greatly appreciated in improving the paper.

[1] T. S. Rappaport, Wireless Communications: Principles and Practice, 2nd Edition, Prentice Hall, 2002.

[2] A. Molisch, F. Tufvesson, J. Karedal, C. Mecklenbrauker, A survey on vehicle-to-vehicle propagation channels, Wireless Communications, IEEE 16 (6) (2009) 12–22.

[3] L. Bernad, T. Zemen, E. Paier, G. Matz, J. Karedal, N. Czink, F. Tufvesson, M. Hagenauer, A. F. Molisch, C. F. Mecklenbruker, Non-wssus vehicular channel characterization in highway and urban scenarios at 5.2 ghz using the local scattering function, in: in Workshop on Smart Antennas (WSA, 2008, pp. 9–15.

[4] L. Bernado, T. Zemen, F. Tufvesson, A. Molisch, C. Mecklenbrauker, The (in-) validity of the wssus assumption in vehicular radio channels, in: Personal Indoor and Mobile Radio Communications (PIMRC), 2012 IEEE 23rd International Symposium on, 2012, pp. 1757–1762.

[5] C. Tepedelenlioglu, A. Abdi, G. Giannakis, The ricean k factor: Estimation and performance analysis, IEEE Transactions on Wireless Communications 24 (5) (2003) 799–810. doi:10.1109/TWC.2003.814338.

[6] G. Azemi, B. Senadji, B. Boashash, Ricean K-Factor estimation in mobile communication systems, IEEE Communications Letters 8 (10) (2004) 617–619. doi:10.1109/LCOMM.2004.835344.

[7] L. Bernado, T. Zemen, J. Karedal, A. Paier, A. Thiel, O. Klemp, N. Czink, F. Tufvesson, A. Molisch, C. Mecklenbräuker, Multi-dimensional k-factor analysis for v2v radio channels in open sub-urban street crossings, in: Personal Indoor and Mobile Radio Communications (PIMRC), 2010 IEEE 21st International Symposium on, 2010, pp. 58–63.

[8] L. Bernadó, T. Zemen, F. Tufvesson, A. F. Molisch, C. F. Mecklenbräuker, Time-, frequency-, and space-varying k-factor of non-stationary vehicular channels for safety relevant scenarios, CoRR abs/1306.3914.

[9] G. Messier, J. Hartwell, An empirical model for nonstationary ricean fading, IEEE Transactions on Vehicular Technology 58 (1) (2009) 14–20. doi:10.1109/TVT.2008.924988.

[10] T. Aulin, A modified model for the fading signal at a mobile radio channel, Vehicular Technology, IEEE Transactions on 28 (3) (1979) 182–203.

[11] E. Ostlin, H.-J. Zepernick, H. Suzuki, A. Pollok, Analysis of correlation between ricean k-factor and vegetation density surrounding a CDMA mobile terminal, in: 1st International Symposium on Wireless Communication Systems, IEEE, 2004, pp. 61–65. doi:10.1109/ISWCS.2004.1407209.

[12] L. Bernado, T. Zemen, A. Paier, J. Karedal, B. Fleury, Parametrization of the local scattering function estimator for vehicular-to-vehicular channels, in: Vehicular Technology Conference Fall (VTC 2009-Fall), 2009 IEEE 70th, 2009, pp. 1–5.

[13] J. Karedal, F. Tufvesson, N. Czink, A. Paier, C. Dumard, T. Zemen, C. Mecklenbrauker, A. Molisch, A geometry-based stochastic mimo model for vehicle-to-vehicle communications, Wireless Communications, IEEE Transactions on 8 (7) (2009) 3646–3657.

[14] D. Krajzewicz, E. Nicolay, M. Behrisch, SUMO - simulation of urban mobility (2011).
URL `http://sumo.sourceforge.net/`

[15] O. Renaudin, V.-M. Kolmonen, P. Vainikainen, C. Oestges, Wideband measurement-based modeling of inter-vehicle channels in the 5-ghz band, Vehicular Technology, IEEE Transactions on 62 (8) (2013) 3531–3540.

[16] C. Cooper, A. Mukunthan, M. Ros, D. Franklin, M. Abolhasan, Dynamic environmental fading in urban vanets, in: Communications (ICC), 2014 IEEE International Conference on, 2014, pp. 5641–5646.

[17] OSM - open street maps.
URL `http://www.openstreetmap.org/`

[18] J. Nuckelt, D. Rose, T. Jansen, T. Kurner, On the use of openstreetmap data for v2x channel modeling in urban scenarios, in: Antennas and Propagation (EuCAP), 2013 7th European Conference on, 2013, pp. 3984–3988.

[19] J. Nuckelt, T. Abbas, F. Tufvesson, C. Mecklenbrauker, L. Bernado, T. Kurner, Comparison of ray tracing and channel-sounder measurements for vehicular communications, in: Vehicular Technology Conference (VTC Spring), 2013 IEEE 77th, 2013, pp. 1–5.

[20] J. Jemai, T. Kumer, A. Varone, J. Wagen, Determination of the permittivity of building materials through WLAN measurements at 2.4 GHz, in: IEEE 16th International Symposium on Personal, Indoor and Mobile Radio Communications, Vol. 1, IEEE, 2005, pp. 589–593. doi:10.1109/PIMRC.2005.1651504.

[21] C. Grosvenor, R. Johnk, J. Baker-Jarvis, M. Janezic, B. Riddle, Time-Domain Free-Field measurements of the relative permittivity of building materials, IEEE Transactions on Instrumentation and Measurement 58 (7) (2009) 2275–2282. doi:10.1109/TIM.2009.2013916.

[22] L. Greenstein, D. Michelson, V. Erceg, Moment-method estimation of the ricean k-factor, IEEE Communications Letters 3.

[23] A. Mukunthan, C. Cooper, D. Franklin, M. Abolhasan, F. Safaei, Studying the impact of the CORNER propagation model on VANET routing in urban environments, in: Vehicular Technology Conference, 2012. VTC Fall 2012. IEEE 76th, IEEE VTS, Quebec City, 2012, pp. 1–5.

[24] A. Varga, OMNeT++ (2009).
URL `http://www.omnetpp.org/`

[25] C. Sommer, Veins (Vehicles in network simulation) (2010).
URL `http://veins.car2x.org/`

[26] E. Giordano, R. Frank, G. Pau, M. Gerla, CORNER: a radio propagation model for VANETs in urban scenarios, Proceedings of the IEEE 99 (7) (2011) 1280–1294.

[27] E. Giordano, R. Frank, G. Pau, M. Gerla, CORNER: a realistic urban propagation model for VANET, in: Seventh International Conference on Wireless On-demand Network Systems and Services (WONS), IEEE, 2010, pp. 57–60.

[28] A. Mukunthan, C. Cooper, D. Franklin, M. Abolhasan, F. Safaei, M. Ros, Experimental validation of the corner propagation model based on signal power measurements in a vehicular environment, in: IEEE WCNC 2013, IEEE WCNC, Shanghai, 2013.

[29] J. Blum, A. Eskandarian, L. Hoffman, Challenges of intervehicle ad hoc networks, IEEE Trans. Intell. Transport. Syst. 5 (4) (2004) 347–351.

[30] G. L. Stber, Principles of Mobile Communication, 2nd Edition, Kluwer Academic Publishers, 2002.

[31] O. Renaudin, V. Kolmonen, P. Vainikainen, C. Oestges, Non-stationary narrowband mimo inter-vehicle channel characterization in the 5-ghz band, Vehicular Technology, IEEE Transactions on 59 (4) (2010) 2007–2015.

[32] O. Renaudin, V. Kolmonen, P. Vainikainen, C. Oestges, Wideband mimo car-to-car radio channel measurements at 5.3 ghz, in: Vehicular Technology Conference, 2008. VTC 2008-Fall. IEEE 68th, 2008, pp. 1–5.

[33] L. C. Andrews, R. L. Phillips, Laser Beam Propagation Through Random Media, 2nd Edition, International Society for Optical Engineering, 2005.

[34] R. He, A. F. Molisch, F. Tufvesson, Z. Zhong, B. Ai, T. Zhang, Vehicle-to-vehicle channel models with large vehicle obstructions, in: Communications, 2014. ICC '14. IEEE International Conference on, 2014.

[35] P.-J. Wang, C.-M. Li, H.-J. Li, Influence of the shadowing on the information transmission distance in inter-vehicle communications, in: IEEE 20th International Symposium on Personal, Indoor and Mobile Radio Communications, IEEE, 2009, pp. 3015–3019. doi:10.1109/PIMRC.2009.5450288.

[36] C. Mecklenbrauker, A. Molisch, J. Karedal, F. Tufvesson, A. Paier, L. Bernado, T. Zemen, O. Klemp, N. Czink, Vehicular channel characterization and its implications for wireless system design and performance, Proceedings of the IEEE 99 (7) (2011) 1189–1212.

[37] S. Bai, D. Nicol, Acceleration of wireless channel simulation using gpus, in: Wireless Conference (EW), 2010 European, 2010, pp. 841 –848. doi:10.1109/EW.2010.5483525.

[38] J. Becerra, J. Nazabal, V. Torres, F. Esparza, M. Navarro, M. Beruete, C. Fernandez, F. Falcone, Wireless channel modeling for campus sensor networks, in: Antenna Technology and Applied Electromagnetics the American Electromagnetics

Conference (ANTEM-AMEREM), 2010 14th International Symposium on, 2010, pp. 1 –4.

[39] D. Olivadese, F. Berizzi, A. Cacciamano, A. Capria, A radar oriented ionospheric channel model based on ray-tracing theory, in: Radar Conference (EuRAD), 2010 European, 2010, pp. 105 –108.